

High-field magnetic properties of the alternating ferro-antiferromagnetic spin-chain compound $\text{Cu}_2(\text{OH})_3\text{Br}$

K. Yu. Povarov,^{1,*} Y. Skourskii,¹ J. Wosnitza,^{1,2} D. E. Graf,³ Z. Zhao,^{4,†} and S. A. Zvyagin^{1,‡}

¹*Dresden High Magnetic Field Laboratory (HLD-EMFL) and Würzburg-Dresden Cluster of Excellence ct.qmat, Helmholtz-Zentrum Dresden-Rossendorf (HZDR), 01328 Dresden, Germany*

²*Institut für Festkörper- und Materialphysik, Technische Universität Dresden, 01062 Dresden, Germany*

³*National High Magnetic Field Laboratory, Tallahassee, Florida 32310, USA*

⁴*State Key Laboratory of Structural Chemistry, Fujian Institute of Research on the Structure of Matter, Chinese Academy of Sciences, Fuzhou, Fujian 350002, People's Republic of China*

(Dated: December 17, 2024)

We present comprehensive high magnetic field studies of the alternating weakly coupled ferro-antiferromagnetic (FM-AFM) spin-1/2 chain compound $\text{Cu}_2(\text{OH})_3\text{Br}$, with the structure of the natural mineral botallackite. Our measurements reveal a broad magnetization plateau at about half of the saturation value, strongly suggesting that the FM chain sublattice becomes fully polarized, while the AFM chain sublattice remains barely magnetized, in magnetic fields at least up to 50 T. We confirm a spin-reorientation transition for magnetic fields applied in the ac^* -plane, whose angular dependence is described in the framework of the mean-field theory. Employing high-field THz spectroscopy, we reveal a complex pattern of high-frequency spinon-magnon bound-state excitations. On the other hand, at lower frequencies we observe two modes of antiferromagnetic resonance, as a consequence of the long-range magnetic ordering. We demonstrate that applied magnetic field tends to suppress the long-range magnetic ordering; the temperature-field phase diagram of the phase transition is obtained for magnetic fields up to 14 T for three principal directions (a , b , c^*).

I. INTRODUCTION

Natural minerals featuring triangular motifs in $S = 1/2$ Cu^{2+} ion arrangements are attracting significant attention [1]. Prominent examples include the frustrated spin-chain linearite [2–5], the spin-liquid candidate herbertsmithite [6–8], the delta-chain material atacamite [9], and the three-leg ladder system antlerite [10, 11], to name a few. Since the triangular-like geometry of magnetic correlations implies competing interactions and the frustration [12, 13], such materials often demonstrate diverse and complex magnetic properties.

$\text{Cu}_2(\text{OH})_3\text{Br}$ (hereafter COHB) is a sister compound of the natural mineral botallackite $\text{Cu}_2(\text{OH})_3\text{Cl}$, which has been recently identified as a new spin-1/2 chain quantum system with a triangular motif of exchange couplings [14–16]. Employing inelastic neutron scattering, Zhang *et al.* [15] has established the presence of alternating and weakly coupled ferromagnetic (FM) and antiferromagnetic (AFM) chains as the key feature of the COHB magnetic structure. Remarkably, the neutron scattering has revealed signatures of the co-existing two-spinon continuum and FM magnons (as well as magnon-spinon bound states resulting from the interaction between FM and AFM chain sublattices) [15]. It was suggested that frustrated interactions between the chains of different types is the specific feature of COHB, leading to intricate ground state and magnetic excitations.

It is worthwhile to mention that not much is known about high-magnetic-field properties of COHB, including its magnetic phase diagram and the high-field spin dynamics. The most important finding in this regards is the field-induced spin-reorientation phase transition in the magnetically ordered state below $T_N = 9.3$ K, with magnetic field applied in the ac plane and $\mu_0 H_c$ between approximately 4.5 and 5 T (for a and c^* directions) [14, 17]. It was shown by the electron spin resonance (ESR spectroscopy) that this discontinuous phase transition is accompanied by a partial softening of a gapped resonance mode [17]. The exact nature of the transition remains an open question. In this work, employing high-field magnetization, tunnel-diode-oscillator (TDO) susceptibility, and ESR spectroscopy techniques, we study magnetic properties of COHB. This allows us to reveal several important features of its high-field behavior, originating from the interplay between the FM and AFM chain sublattices.

II. CRYSTAL AND MAGNETIC STRUCTURE

COHB crystallizes in the monoclinic structure with space group $P2_1/m$ and lattice parameters $a = 5.63$ Å, $b = 6.12$ Å, $c = 5.72$ Å, $\beta = 93.1^\circ$, and $Z = 4$ [18, 19]. A schematic view of the COHB crystal structure is shown in Fig. 1(a). There are two types of spin chains, with sites Cu1 and Cu2, respectively. The chains are arranged in well-separated layers in the ab plane, running along the b direction.

Neutron diffraction in COHB below $T_N = 9.3$ K revealed a peculiar spin order with the propagation vector $\mathbf{Q} = (1/2, 0, 0)$ [15]. It was shown that along the b axis,

* k.povarov@hzdr.de

† zhiyingzhao@fjirm.ac.cn

‡ s.zvyagin@hzdr.de

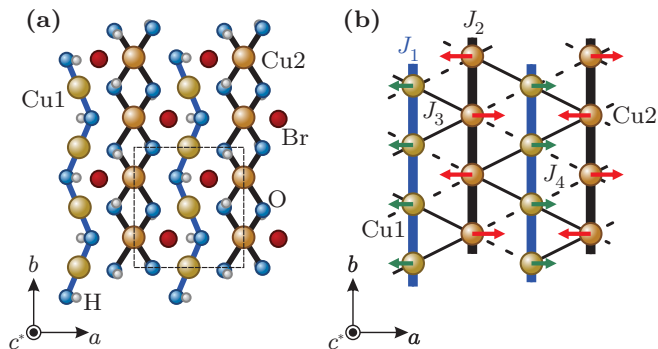


FIG. 1. (a) Schematic view of the crystal structure of COHB. Orange spheres represent the Cu^{2+} ions; blue, red, and grey ones stand for O, Br, and H atoms, correspondingly. The dashed line shows the unit cell. Cu1 ions form ferromagnetic chains, and Cu2 ions form antiferromagnetic chains. (b) Schematic view of the magnetic structure of COHB. The projections of the Cu spins in the ab plane (following [15]) are indicated by arrows. Thick blue lines, thick black lines, thin solid lines, and thin dashed lines correspond to exchange interactions J_1 , J_2 , J_3 , and J_4 respectively.

Cu1 spins are aligned ferromagnetically with spins oriented nearly along the diagonal direction in the ac plane, while Cu2 spins are aligned antiferromagnetically with spins oriented along the a axis [Fig. 1(b)].

As follows from Ref. [16], the intrachain exchange interactions are $J_1/k_B = -16.2$ K and $J_2/k_B = 55.7$ K (for FM and AFM chains, respectively), while the interchain exchange interactions are $J_3/k_B = 9.3$ K and $J_4/k_B = 4.6$ K [see Fig. 1(b)]. These values are in line with estimates given in Ref. [15].

III. EXPERIMENTAL

Single crystals of COHB were grown using a conventional hydrothermal method, as described in Ref. [14]. We measured the magnetization in DC fields up to 14 T using a vibrating sample magnetometer (VSM) (product of Quantum Design, Inc.). For pulsed-field magnetization measurements, we used a coaxial pick-up coil magnetometer (PUCM), similar to that described in Ref. [20]. We measured the high-frequency susceptibility in DC fields up to 41.5 T using a TDO magnetometer [21–23]. In our ESR experiments, we employed a THz-range spectrometer (similar to the one described in Ref. [24]), equipped with a 16 T superconducting magnet. We used VDI microwave-chain sources (product of Virginia Diodes, Inc., USA) and backward wave oscillators (product of NPP Istok, Russian Federation) to generate radiation in the frequency range of 50 – 900 GHz. A hot-electron n-InSb bolometer (product of QMC Instruments Ltd., UK), operated at 4.2 K, was employed as a THz detector. For the ESR experiments we used a probe in the Voigt geometry for $H \parallel a$ and b , while for $H \parallel c^*$ we used the Faraday geometry. We used 2,2-diphenyl-

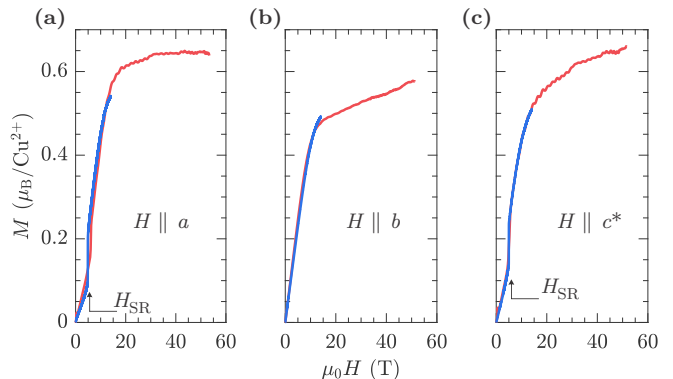


FIG. 2. (a)-(c) Magnetization of COHB single crystals for magnetic fields applied along the a , b and c^* directions, respectively. Blue lines are the data, obtained at $T = 2$ K using VSM up to 14 T; red lines correspond to pulsed-field magnetization data at $T = 1.5$ K, obtained employing PUCM up to 55 T. The arrows mark the spin-reorientation transition field H_{SR} .

1-picrylhydrazyl (DPPH) as a standard frequency-field marker. The crystals were oriented with $\pm 5^\circ$ accuracy.

IV. HIGH-FIELD MAGNETIZATION

In Fig. 2, we present magnetization results for $H \parallel a, b, c^*$. For $H \parallel a, c^*$, we observe magnetization steps at $\mu_0 H_{\text{SR}} \simeq 4.9$ T and 5 T, respectively. These discontinuities corresponds to the spin-reorientation transition, which was previously reported by Zhao *et al.* [14]. No steps appear for $H \parallel b$. In addition, at higher fields, we observe a broad plateau at half of the nominal full magnetization (that would be close to one Bohr magneton μ_B per Cu^{2+}), suggesting that half of the Cu^{2+} ions are polarized. This effective 1/2-magnetization plateau begins to develop around 10 – 15 T and is visible up to 55 T. Since the mutual orientation of FM chain sublattices appears to be defined by smaller exchange couplings $J_{3,4}/k_B < 10$ K, it is evident that the magnetic field drives the FM chain sublattice to the full saturation first, leaving, on the other hand, the AFM chain sublattice with $J_2/k_B \simeq 60$ K only barely magnetized in this field range.

V. MAGNETIC PHASE DIAGRAM

In Figs. 3(a)-(c), we show the angular dependence of the SR transition, observed in COHB below T_N . As revealed from our experiments, the spin-reorientation transition is visible not only for $H \parallel a, c^*$ directions, but for a wide range of angles in ac^* plane. The dependence has a minimum; this field direction corresponds to the easy-axis anisotropy direction for spins in the FM chains sublattice [Fig. 3(d)], as determined by neutron-

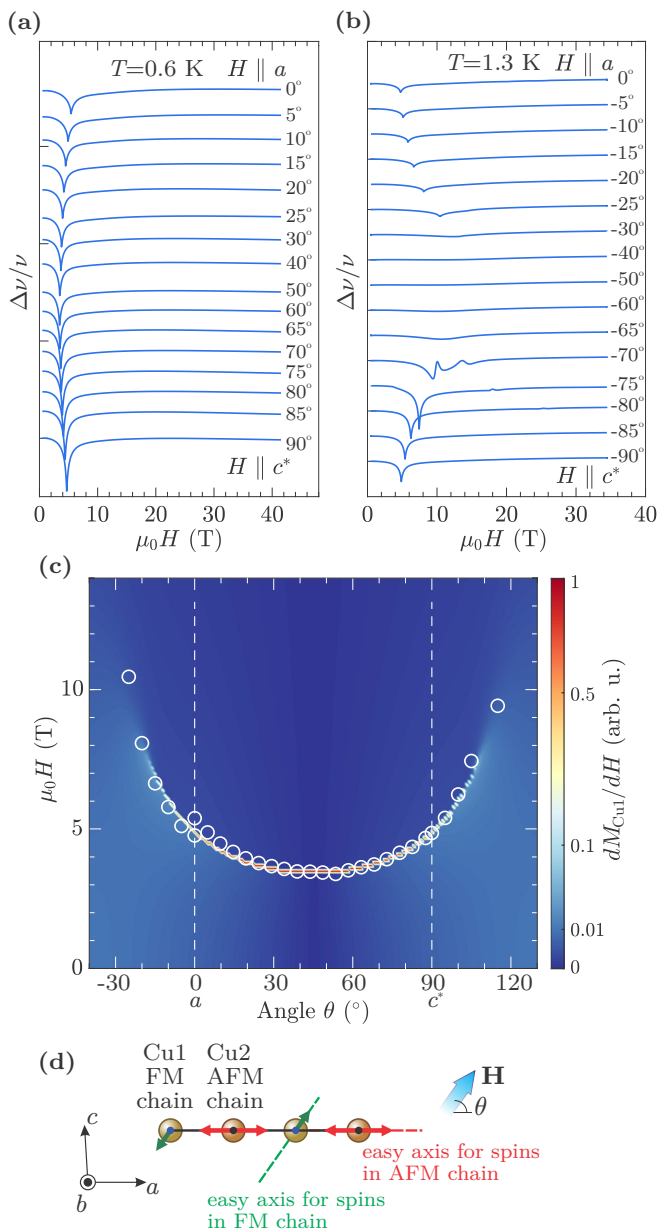


FIG. 3. (a) Relative changes of the TDO-circuit frequency for fields applied between a ($\theta = 0^\circ$) and c^* ($\theta = 90^\circ$) at 0.6 K. (b) Relative change of TDO-circuit frequency for fields applied between a ($\theta = 0^\circ$) and $-c^*$ ($\theta = -90^\circ$) at 1.3 K. (c) Angular dependence of H_{SR} as determined from the TDO anomalies (circles). For comparison, we show the calculated Cu1 chain sublattice spin susceptibility (colormap; see Appendix B). (d) Intrachain anisotropy axes and zero-field spin arrangement in COHB, view along b . Small green and red arrows are spin directions at Cu1 and Cu2 sites, respectively (according to Ref. [15]). Green and red dashed lines show the directions of the easy axes for spins in the corresponding chains (after Ref. [17]). The thick blue arrow represents the external magnetic field.

diffraction measurements [15] and magnetization angular dependence [17]. The present angular dependence is in a good agreement with the one obtained in Ref. [17] and their phenomenological description. For a more detailed analysis of the $H_{\text{SR}}(\theta)$ we also account for interactions between the AFM and FM chain sublattices. In addition to the Heisenberg couplings J_3 and J_4 , we consider possible antisymmetric Dzyaloshinskii–Moriya (DM) interactions [25, 26] between the chains, given as $\hat{\mathcal{H}}_{\text{DM}} = \mathbf{D} \cdot [\hat{\mathbf{S}}_{\text{Cu1}} \times \hat{\mathbf{S}}_{\text{Cu2}}]$. Such interactions (\mathbf{D}_3 on J_3 -type bonds, and \mathbf{D}_4 on J_4 -type bonds) are allowed by the symmetry of COHB, with the corresponding DM vector directions following a complex pattern. Neutron spectroscopy suggests that those contributions can be relatively strong [15]. The DM pattern and the calculation details are described in the Appendices A and B. Here we provide a brief summary. The model assumes fixed orientation of AFM spins, while the FM spins experience a combination of intricate mean-field and the external field. The analysis suggests the following form of the molecular field acting on the FM chains:

$$\pm g\mu_B\mu_0\mathbf{H}_{\text{mol}} = (J_3 - J_4, 0, -D_{3b} - D_{4b}). \quad (1)$$

Here the $D_{3b,4b}$ are the components of the corresponding DM vectors along the b axis. The sign of this molecular field is different for neighboring FM chains. The experimental angular dependence of the spin-reorientation transition field is most correctly reproduced assuming both the easy-axis direction for spins in the FM chains and the field \mathbf{H}_{mol} colaligned at nearly 45° to the a axis. This is the experimentally observed direction of Cu1 spins at zero field [15]. Figure 3(c) shows a comparison of the mean-field model calculations with our experimental TDO data. The calculations yield a J_1 anisotropy parameter (relative increase in interaction strength along the preferred direction) of $\delta \simeq 0.2$, which is in a good agreement with the value $\delta = 0.17$ obtained from linear spin-wave theory [15]. The mean-field model also suggests $(J_3 - J_4)/k_B \simeq 2.5$ K. In the spin-wave analysis of Ref. [15] this difference is about 10 K. Thus, the interchain interactions appear to be more frustrated according to the mean-field estimate. The b components of the DM vectors on these bonds supposedly have a similar magnitude of about $|D_{3b} + D_{4b}|/k_B \simeq 2.5$ K. With these parameters, the FM chains also create a staggered field along a on the AFM sites, providing consistent description of the zero-field magnetic state proposed in Ref. [15].

Now we discuss the phase diagram of COHB in fields above H_{SR} . In Figs. 4(a)–4(c), we show the exemplary temperature dependences of the COHB magnetization for fields applied along the a , b , and c^* axes, respectively. The transition into the magnetically ordered phase is well visible as a cusp in the $M(T)$ curves.

In Figs. 4(d)–4(f), we present a colormap of the temperature derivative of the magnetization dM/dT in magnetic fields $H \parallel a$, b , and c^* , respectively (field step is 1 T). The applied magnetic field suppresses the long-range ordered phase. An asymmetry of the corresponding phase bound-

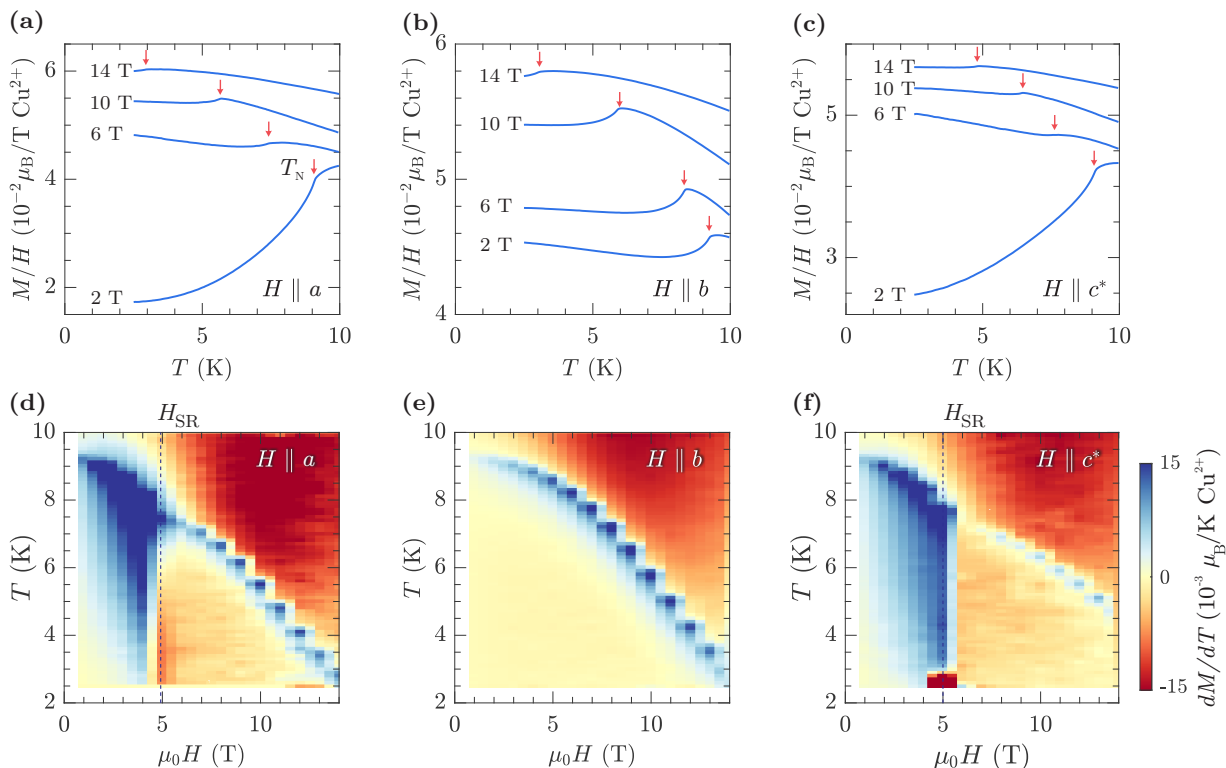


FIG. 4. (a)-(c) Examples of temperature dependencies of the field-normalized magnetization M/H of COHB at 2, 6, 10, and 14 T in magnetic fields $H \parallel a$, b , and c^* , respectively. The arrows indicate anomalies, related to the long-range ordering. The data are offset for clarity. (d)-(f) Colormap of the COHB magnetization derivative with respect to temperature, dM/dT , with the magnetic fields applied along a , b , and c^* , respectively. The magnetic field step is 1 T. Black dashed lines mark the spin-reorientation transition field.

ary between c^* and other field directions is evident from the data present in Fig. 4. This is a very unusual and important observation. It is known that in the presence of staggered terms (such as the DM interactions) the application of magnetic field can result in intricate effective staggered fields [27], affecting interchain spin correlations and thus varying H_c . Such an effect was observed, e.g., in the spin-chain system $\text{CuCl}_2 \cdot 2[(\text{CD}_3)_2\text{SO}]$ [28]. It is likely that similar effects are responsible for the pronounced anisotropy observed in COHB as well.

VI. MAGNETIC EXCITATIONS

In Figs. 5(a)-5(c) we present frequency-field diagrams of magnetic excitations in COHB for $H \parallel a$, b , and c^* , respectively. Corresponding examples of ESR spectra are shown in Figs. 5(d)-5(f). For these three orientations, we observed multiple excitations at relatively high frequencies (labeled as $F_{A1,2}$, $F_{B1,2,3}$, and F_{C1} for $H \parallel a$, b , and c^* , respectively). The excitation frequencies of these resonances decrease with the applied magnetic field in a nearly linear fashion. Linear extrapolations of the frequency-field dependencies of these excitations to $H = 0$ yield 1 THz to 1.2 THz, which agrees with the energy range (4 – 5 meV) for spinon-magnon bound

states at the Γ point revealed by neutron-scattering experiments [15].

Since COHB undergoes a transition into a magnetically ordered state at $T_N = 9.3$ K, below this temperature one would expect the presence of at least two relativistic modes of antiferromagnetic resonance (AFMR). We indeed observed these pseudo-Goldstone modes (low-energy modes M_1 and M_2). Both AFMR modes are gapped ($\Delta_1 = 130 \pm 5$ GHz and $\Delta_2 = 300 \pm 10$ GHz at $T = 1.5$ K, respectively), suggesting the presence of biaxial magnetic anisotropy in COHB. Our observation expands the previous low-frequency results of Xiao *et al.* [17], where only the M_1 and M_3 modes were observed. The low-frequency AFMR mode M_1 exhibits partial softening at H_{SR} , similar as observed for a conventional spin-flop transition in collinear easy-axis antiferromagnets [29]. Above the spin-reorientation transition field, we observe AFMR modes M_3 and M_4 (the latter visible only for $H \parallel c^*$).

In addition to the F-labeled multiplets and M-labeled AFMR modes, we observed a broad and relatively intense mode labeled P with the linear frequency-field dependence [Figs. 5(a) and 5(c)]. This mode appears at frequencies, somewhat higher than the ones of the AFMR modes. The coexistence of AFMR excitations and the mode P in the high-field range can be associ-

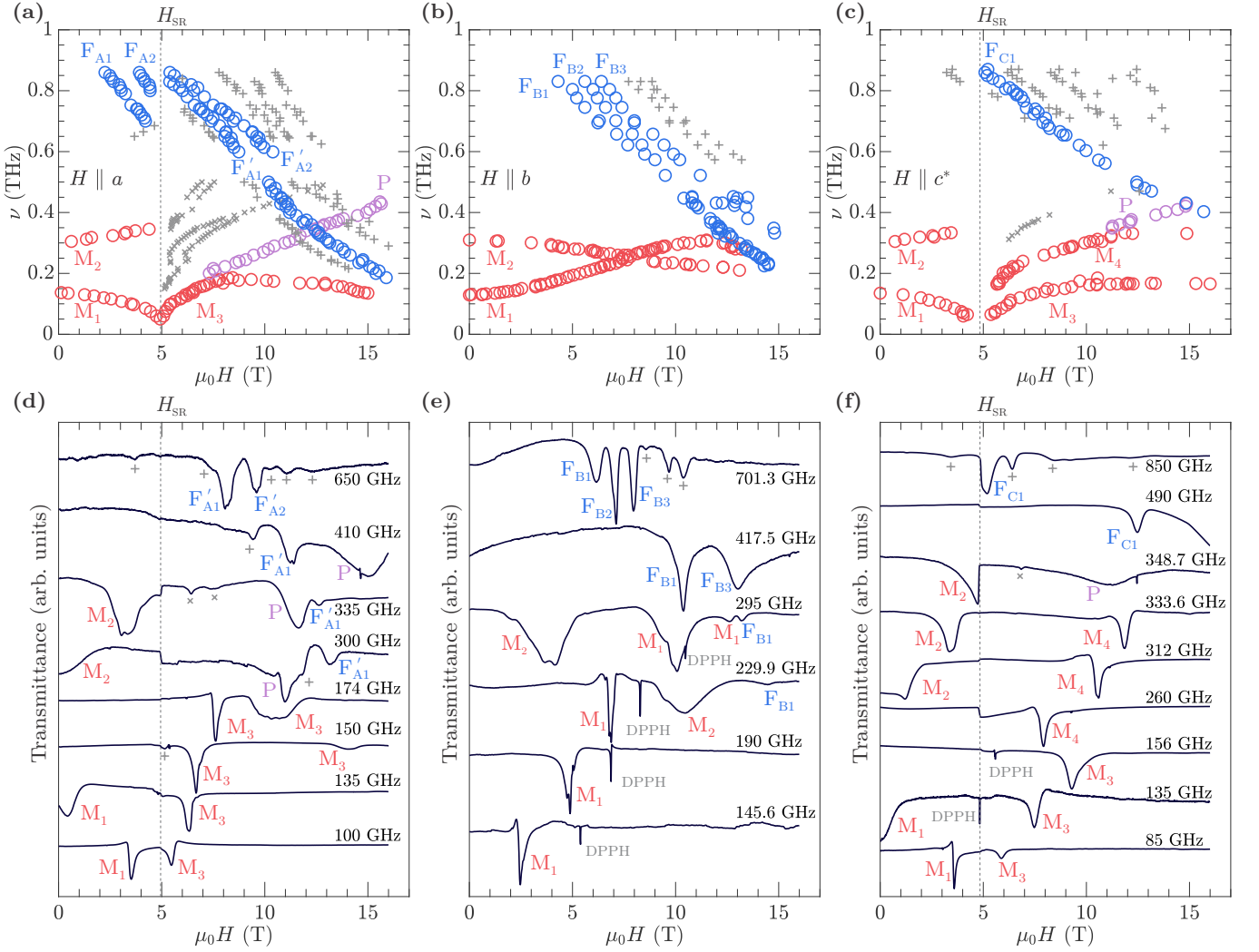


FIG. 5. (a)-(c) Frequency-field diagrams of the ESR excitations in COHB for $H \parallel a, b$, and c^* , respectively ($T = 1.5$ K). Modes M correspond to AFMR (red circles), while modes F correspond to magnon-spinon bound state excitations (blue circles). The modes P correspond to broad resonances at high fields, that is likely related to spinon deconfinement (purple circles). Crosses denote weaker unclassified resonances. (d)-(f) Selected examples of ESR spectra for $H \parallel a, b$, and c^* , respectively. The dashed lines mark the spin-reorientation field H_{SR} .

ated with spinon deconfinement observed in some quasi-one-dimensional quantum antiferromagnets [30–33]. This scenario is possible in COHB, since moderate magnetic fields significantly suppress magnetic order and, thus, enhance the quantum effects [see phase diagrams in Figs. 4(d)-4(f)].

The M and F modes show evidence of intricate interactions, depending on the direction of the magnetic field. In magnetic fields of about 13 - 14 T applied along the a axis signatures of the avoided crossing appear. For $H \parallel b$, above about 12 T, there is evidence for spin-wave damping upon interaction with the multiplet. At high magnetic fields, we also observe a number of weak resonances, labeled with crosses in Fig. 5. Their origin remains an open question.

The correlation of the M modes parameters to the mag-

netic ordering is corroborated by the temperature dependence of the ESR signal. Figure 6(a) shows the temperature and field dependence of the ESR signal corresponding to mode M_1 ($H \parallel b$ at 133 GHz), and Fig. 6(b) of the ESR signal corresponding to mode M_2 ($H \parallel c^*$ at 304.9 GHz). Both modes demonstrate a rapid crossover to the paramagnetic resonance (with $g \sim 2.26$ and 2.03, correspondingly) upon warming. For mode M_1 this can be examined in more detail, since its frequency-field dependence follows a law (at least up to 5 T), typical for AFMR [34]:

$$\nu_1 = \sqrt{\Delta_1^2 + (g\mu_0\mu_B H_{res}/h)^2}, \quad (2)$$

where h is the Planck constant. The temperature dependence of ESR field and linewidth at 133 GHz, and

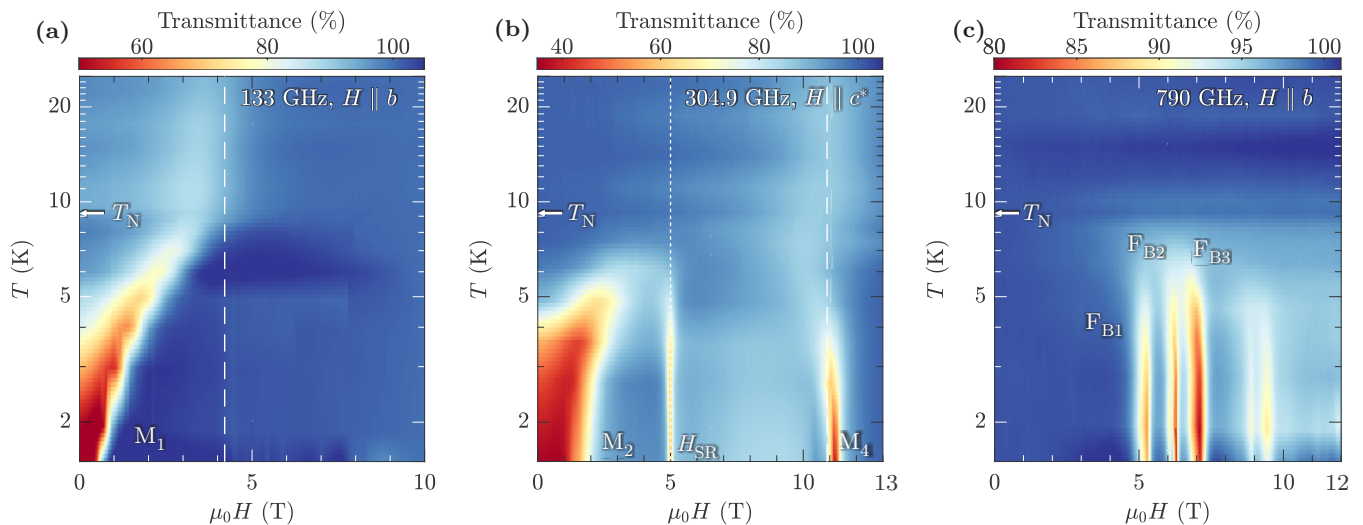


FIG. 6. THz radiation transmittance vs. field and temperature for $\nu = 133$ GHz and $H \parallel b$ (a), $\nu = 304.9$ GHz and $H \parallel c^*$ (b), as well as for $\nu = 790$ GHz and $H \parallel b$ (c). Arrows indicate the zero-field Néel temperature, vertical dashed lines show the paramagnetic resonance position above this temperature, and the vertical dotted line marks the H_{SR} field. The transmittance is normalized to the respective value far away from the resonance field. Note the logarithmic temperature scale.

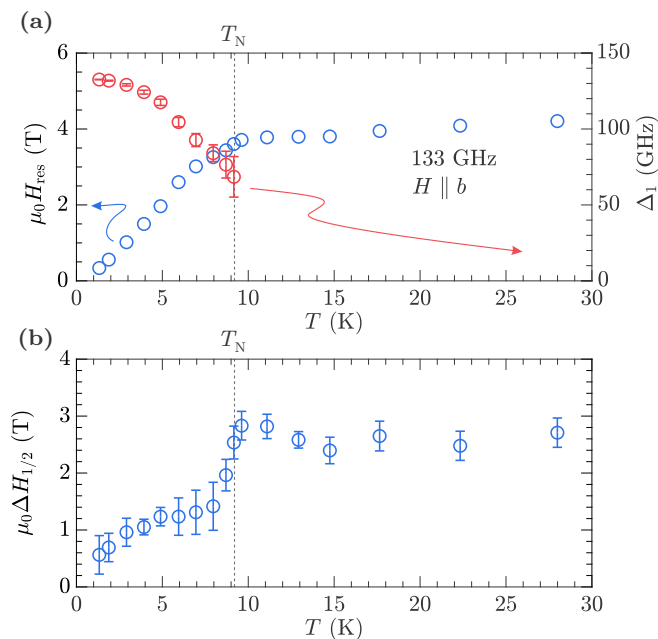


FIG. 7. (a) Temperature dependence of the ESR field (blue, right axis) at 133 GHz, $H \parallel b$, and of the corresponding gap Δ_1 (red, left axis) extracted from the data according to Eq. (2). (b) ESR linewidth at 133 GHz, $H \parallel b$. Dotted line marks the Néel temperature T_N .

the corresponding gap value $\Delta_1(T)$ are shown in Fig. 7. The resonance field decreases rapidly upon cooling below T_N , while the line becomes significantly narrower in the ordered phase. In contrast, at high temperatures, and especially near T_N the line is very broad.

On the other hand, the F modes, resulting from bound

states of spinons and magnons [15], show a largely different temperature dependence, as shown in Fig. 6(c) for $H \parallel b$ at 790 GHz. Without any significant change in the respective position, the F_B resonances just lose the intensity and disappear. The same behavior was observed for the weaker satellite lines. All these lines become invisible at temperatures, corresponding to the energy scale of interchain coupling $J_3/k_B \sim T_N$.

VII. SUMMARY

In summary, we performed systematic high-field magnetization and ESR studies of the alternating FM-AFM spin-1/2 chain compound $\text{Cu}_2(\text{OH})_3\text{Br}$. We observed a magnetization plateau with the magnetic moment close to one-half of the saturation value. This suggests the full polarization of the FM chain sublattice, while the large AFM exchange coupling keeps the AFM chain sublattice only weakly magnetized. We measured the angular dependence of the spin-reorientation transition, evidencing that the spin reorientation occurs within the FM chain sublattice.

Our ESR experiments indicate a very rich excitation spectrum in COHB. In addition to the high-energy multiplet (originating from magnon-spinon interactions) we observed two modes of antiferromagnetic resonance, a consequence of the long-range magnetic ordering below $T_N = 9.3$ K.

On the other hand, we observed a collapse of the magnetically ordered phase in applied magnetic field. We measured the $H - T$ phase diagram for three principal magnetic field directions, revealing the anisotropic nature of the order-disorder phase boundaries. These find-

ings urge for careful accounting of possible small-term components of the COHB spin Hamiltonian, including the Dzyaloshinskii–Moriya components of the interchain couplings.

ACKNOWLEDGMENTS

This work was supported by the Deutsche Forschungsgemeinschaft through the Würzburg-Dresden Cluster of Excellence on Complexity and Topology in Quantum Matter - *ct.qmat* (EXC 2147, project No. 390858490) and the SFB 1143, as well as by HLD at HZDR, member of the European Magnetic Field Laboratory (EMFL). A portion of this work was performed at the National High Magnetic Field Laboratory, which is supported by the National Science Foundation Cooperative Agreement No. DMR-1644779 and the State of Florida. Z.Y.Z. is grateful for the support from the National Natural Science Foundation of China (Grant No. 52072368). We thank M. Uhlarz (HZDR) for assistance with the PPMS system.

Note Added. Recently we became aware of the work of Reinold *et al.* [35], who studied the phase diagram of COHB for magnetic fields applied along the chain direction and observed a field-induced collapse of the magnetic order with $T_N = 9.3$ K. This finding is in line with our results.

Appendix A: Interchain Dzyaloshinskii–Moriya interactions in COHB

In Fig. 8(a) we present the pattern of the possible interchain DM interactions in COHB (the symmetry analysis was performed with the help of *SpinW* package [36]). The bonds J_3 and J_4 host the DM interactions \mathbf{D}_3 and \mathbf{D}_4 correspondingly. The symmetry of COHB allows all components of the DM vector on these bonds. Both, \mathbf{D}_3 and \mathbf{D}_4 , exist in two variants, differing by the sign of the a and c components (we always assume the bonds being “directed” from the Cu1 sites towards the Cu2 sites):

$$\begin{aligned} \mathbf{D}_3 &= (D_{3a}, -D_{3b}, D_{3c}), \\ \mathbf{D}'_3 &= (-D_{3a}, -D_{3b}, -D_{3c}), \\ \mathbf{D}_4 &= (D_{4a}, D_{4b}, D_{4c}), \\ \mathbf{D}'_4 &= (-D_{4a}, D_{4b}, -D_{4c}). \end{aligned} \quad (\text{A1})$$

Appendix B: Mean-field model for spin reorientation in COHB

We consider the influence of the AFM chain sublattice on the FM chains. Let us start with writing down the interactions acting on the Cu1 site I in the FM chain, as

illustrated in Fig. 8(a). The corresponding spin Hamiltonian is:

$$\begin{aligned} \hat{\mathcal{H}}_I &= \hat{\mathcal{H}}_{\text{intrachain}} + J_3 \hat{\mathbf{S}}_I \cdot (\hat{\mathbf{S}}_1 + \hat{\mathbf{S}}_4) + J_4 \hat{\mathbf{S}}_I \cdot (\hat{\mathbf{S}}_2 + \hat{\mathbf{S}}_3) \\ &\quad - \mathbf{D}_3 \cdot [\hat{\mathbf{S}}_I \times (\hat{\mathbf{S}}_1 + \hat{\mathbf{S}}_4)] - \mathbf{D}'_4 \cdot [\hat{\mathbf{S}}_I \times (\hat{\mathbf{S}}_2 + \hat{\mathbf{S}}_3)]. \end{aligned} \quad (\text{B1})$$

We replace the spin operators related to the AFM Cu2 ions with the corresponding expectation values:

$$\langle \hat{\mathbf{S}}_1 \rangle = \langle \hat{\mathbf{S}}_4 \rangle = \begin{pmatrix} -S \\ 0 \\ 0 \end{pmatrix}, \quad \langle \hat{\mathbf{S}}_2 \rangle = \langle \hat{\mathbf{S}}_3 \rangle = \begin{pmatrix} S \\ 0 \\ 0 \end{pmatrix}.$$

The combination of the strong J_2 exchange and its easy-axis anisotropy (a as preferred direction) completely fixes the staggered arrangement of the Cu2 spins. Possible effects of the magnetic field on these spins are neglected, as we are considering the small-field limit only. The resulting version of the Hamiltonian (B1) reads as:

$$\begin{aligned} \hat{\mathcal{H}}_I &= \hat{\mathcal{H}}_{\text{intrachain}} - \hat{\mathbf{S}}_I \cdot \begin{pmatrix} 2S \\ 0 \\ 0 \end{pmatrix} (J_3 - J_4) \\ &\quad + \hat{\mathbf{S}}_I \cdot \begin{pmatrix} 2S \\ 0 \\ 0 \end{pmatrix} \times (\mathbf{D}_3 - \mathbf{D}'_4). \end{aligned} \quad (\text{B2})$$

The last two terms are equivalent to the effective molecular field:

$$g\mu_B\mu_0 \mathbf{H}_I^{\text{mol}} = 2S \begin{pmatrix} J_3 - J_4 \\ -D_{3c} - D_{4c} \\ -D_{3b} - D_{4b} \end{pmatrix}. \quad (\text{B3})$$

This is the effective field experienced by Cu1 on site I of the FM chain. The molecular field at site II is obtained by replacing $\mathbf{D}_3 \rightarrow \mathbf{D}'_3$ and $\mathbf{D}'_4 \rightarrow \mathbf{D}_4$ [as follows from the bond scheme in Fig. 8(a)]:

$$g\mu_B\mu_0 \mathbf{H}_{II}^{\text{mol}} = 2S \begin{pmatrix} J_3 - J_4 \\ D_{3c} + D_{4c} \\ -D_{4b} - D_{3b} \end{pmatrix} \quad (\text{B4})$$

Thus, the effective molecular field experienced by the Cu1 spins in the FM chains consists of a uniform component in the ac plane and staggered component along b . Between neighboring FM chains these fields would be given by replacing $S \rightarrow -S$. Since there is no reports of a staggered spin component within the FM chains, we will assume the D_c components to be negligible. This leaves only the uniform part of \mathbf{H}^{mol} , with the sign alternating between neighboring FM chains. This leads to the Cu1 spin arrangement as proposed for the zero-field structure [15].

The intrachain Hamiltonian from Eq. (B1) can be written as:

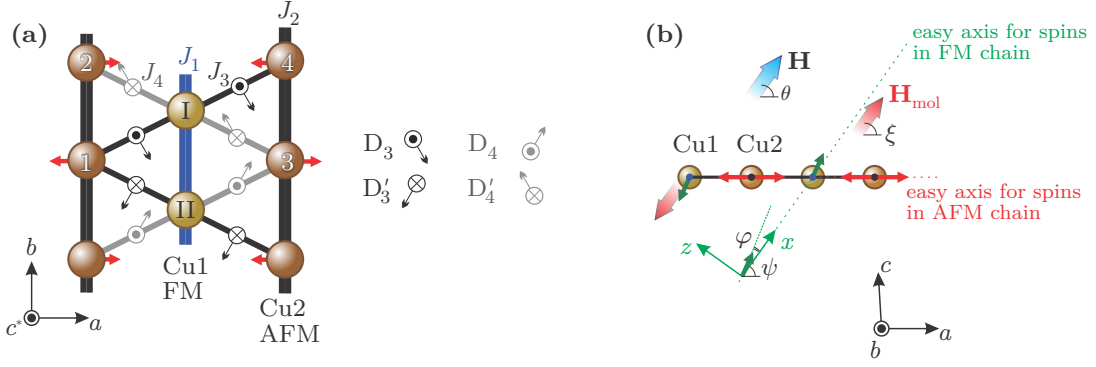


FIG. 8. (a) Mean-field theory scheme for the Cu1 sites in the FM chain subsystem. The red arrows show the directions of the spins in the AFM chains. Blue and black bars represent ferromagnetic J_1 and antiferromagnetic J_2 couplings, respectively. Interchain interactions J_3 and J_4 are denoted by the black and gray line segments; arrows are the DM vectors. (b) Details of the mean-field model geometry in ac^* projection (see the text for angle definitions).

$$\hat{\mathcal{H}}_{\text{intrachain}} = \sum_{\alpha, \beta=x, y, z} 2J_1^{\alpha\beta} \hat{S}_I^\alpha \cdot \langle \hat{S}_{II}^\beta \rangle. \quad (\text{B5})$$

Here, $\langle \hat{S}_{II}^\beta \rangle$ is the spin expectation value for site I's neighbors within the chain. Thus, the full Hamiltonian of a single Cu1 spin is:

$$\hat{\mathcal{H}}_I = \sum_{\alpha, \beta} 2J_1^{\alpha\beta} \hat{S}_I^\alpha \cdot \langle \hat{S}_{II}^\beta \rangle - g\mu_B\mu_0(\mathbf{H} \pm \mathbf{H}_{\text{mol}})\hat{S}_I. \quad (\text{B6})$$

Here, the \pm sign of the interchain molecular field refers to neighboring chains.

Let us assume that the local anisotropy axis of the FM chain lies within the ac plane, at an angle ψ with respect to the a direction of the crystal. We select this direction as x , b as y , and complement it with the orthogonal direction z . In this reference frame, the J_1 tensor is

$$J_1^{\alpha\beta} = J_1 \begin{pmatrix} 1 + \delta & 0 & 0 \\ 0 & 1 & 0 \\ 0 & 0 & 1 \end{pmatrix}, \quad (\text{B7})$$

and the effective interchain field is

$$\mathbf{H}_{\text{mol}} = H_{\text{mol}} \begin{pmatrix} \cos(\psi - \xi) \\ 0 \\ -\sin(\psi - \xi) \end{pmatrix}. \quad (\text{B8})$$

Here, $\tan \xi = (-D_{3b} - D_{4b})/(J_3 - J_4)$ is the effective field angle, resulting from the interplay of the DM interactions and symmetric exchange, and $H_{\text{mol}} = 2S(g\mu_B\mu_0)^{-1}\sqrt{(J_3 - J_4)^2 + (D_{3b} + D_{4b})^2}$ is the corresponding molecular field magnitude. Let the external field be aligned at an angle θ to the a -axis in the ac plane, written as:

$$\mathbf{H} = H \begin{pmatrix} \cos(\psi - \theta) \\ 0 \\ -\sin(\psi - \theta) \end{pmatrix} \quad (\text{B9})$$

in the xyz reference frame. Finally, the spin operators in the semiclassical approximation are

$$\hat{S}_{I,II} = \langle \hat{S}_{I,II} \rangle = S \begin{pmatrix} \cos \varphi \\ 0 \\ \sin \varphi \end{pmatrix}, \quad (\text{B10})$$

with the angle φ characterizing the possible tilt away from the anisotropy axis x . Thus, the Hamiltonian (B6) corresponds to the energy:

$$E_{\pm}(\varphi) = -2J_1S^2 - 2J_1S^2\delta \cos^2 \varphi \pm g\mu_B\mu_0H_{\text{mol}}S \cos(\varphi + \psi - \xi) - g\mu_B\mu_0HS \cos(\psi + \varphi - \theta), \quad (\text{B11})$$

with different H_{mol} sign for neighboring chains.

We consider independent φ angles for neighboring chains, φ_+ and φ_- , respectively. Then, the full energy we need to minimize is:

$$E(\varphi_+, \varphi_-) = E_+(\varphi_+) + E_-(\varphi_-). \quad (\text{B12})$$

This energy can be minimized for a given external field and a set of intrinsic parameters $2J_1\delta$, H_{mol} , ψ , and ξ .

Thus, we can determine the optimal spin configuration in the FM chains and obtain the magnetization curve for the Cu1 chain sublattice. In Fig. 5(c) of the main text we show the experimentally measured H_{SR} field as function of orientation, overlaid with the spin susceptibility in the Cu1 chain sublattice, which is $-d^2E/dH^2$ derivative of the energy Eq. (B12) at optimal values of angles φ_+ , φ_- .

For a good agreement with the COHB data, both angles ψ and ξ need to be close to 45° . The minimum in $H_{\text{SR}}(\theta)$ is located at $\theta \simeq \psi$. Thus, the experimentally found minimum at 45° determines the orientation of the intrachain anisotropy axis. The angle ξ (and, hence, strength of the DM interaction) has a more subtle effect. A molecular field pointing away from the intrachain anisotropy axis direction keeps the critical-field minimum near $\theta = \psi$, but makes the $H_{\text{SR}}(\theta)$ dependence asymmet-

ric with respect to this angle. Hence, only $\xi \simeq 45^\circ$ (and, consequently, nearly equal contributions from Heisenberg and DM interactions) allows a good agreement with the nearly-symmetric angular dependence obtained experimentally.

We find that experimental $H_{\text{SR}}(\theta)$ is best fit with the effective parameters $2S^2|J_1|\delta/k_B \simeq 3.2$ K and $g\mu_B\mu_0H_{\text{mol}}/k_B \simeq 3.5$ K, with both $\xi \simeq \psi \simeq 45^\circ$. This is consistent with $J_1/k_B = -30$ K and $\delta = 0.17$ from linear spin-wave theory [15]. The difference $(J_3 - J_4)/k_B$ is roughly the same as sum $|D_{3b} + D_{4b}|/k_B$, both of them being about 2.5 K. The sign of $D_{3b} + D_{4b}$ should be negative; then the direction of the molecular field would fully align with the direction of the anisotropy axis at J_1 bond. Reversely, the staggered molecular field experienced by the spins in the AFM chain would be strictly along a in that case.

-
- [1] D. Inosov, Quantum magnetism in minerals, *Adv. Phys.* **67**, 149 (2018).
- [2] B. Willenberg, M. Schäpers, K. C. Rule, S. Süllow, M. Reehuis, H. Ryll, B. Klemke, K. Kiefer, W. Schottenhamel, B. Büchner, B. Ouladdiaf, M. Uhlarz, R. Beyer, J. Wosnitza, and A. U. B. Wolter, Magnetic Frustration in a Quantum Spin Chain: The Case of Linarite $\text{PbCuSO}_4(\text{OH})_2$, *Phys. Rev. Lett.* **108**, 117202 (2012).
- [3] B. Willenberg, M. Schäpers, A. U. B. Wolter, S.-L. Drechsler, M. Reehuis, J.-U. Hoffmann, B. Büchner, A. J. Studer, K. C. Rule, B. Ouladdiaf, S. Süllow, and S. Nishimoto, Complex Field-Induced States in Linarite $\text{PbCuSO}_4(\text{OH})_2$ with a Variety of High-Order Exotic Spin-Density Wave States, *Phys. Rev. Lett.* **116**, 047202 (2016).
- [4] K. Yu. Povarov, Y. Feng, and A. Zheludev, Multiferroic phases of the frustrated quantum spin-chain compound linarite, *Phys. Rev. B* **94**, 214409 (2016).
- [5] E. Cemal, M. Enderle, R. K. Kremer, B. Fåk, E. Ressouche, J. P. Goff, M. V. Gvozdikova, M. E. Zhitomirsky, and T. Ziman, Field-induced States and Excitations in the Quasicritical Spin-1/2 Chain Linarite, *Phys. Rev. Lett.* **120**, 067203 (2018).
- [6] P. Mendels, F. Bert, M. A. de Vries, A. Olariu, A. Harrison, F. Duc, J. C. Trombe, J. S. Lord, A. Amato, and C. Baines, Quantum Magnetism in the Paratacamite Family: Towards an Ideal Kagomé Lattice, *Phys. Rev. Lett.* **98**, 077204 (2007).
- [7] M. R. Norman, Colloquium: Herbertsmithite and the search for the quantum spin liquid, *Rev. Mod. Phys.* **88**, 041002 (2016).
- [8] Q. Barthélemy, A. Demuer, C. Marcenat, T. Klein, B. Bernu, L. Messio, M. Velázquez, E. Kermarrec, F. Bert, and P. Mendels, Specific Heat of the Kagome Antiferromagnet Herbertsmithite in High Magnetic Fields, *Phys. Rev. X* **12**, 011014 (2022).
- [9] L. Heinze, H. O. Jeschke, I. I. Mazin, A. Metavitsiadis, M. Reehuis, R. Feyherherm, J.-U. Hoffmann, M. Bartkowiak, O. Prokhnenko, A. U. B. Wolter, X. Ding, V. S. Zapf, C. Corvalán Moya, F. Weickert, M. Jaime, K. C. Rule, D. Menzel, R. Valentí, W. Brenig, and S. Süllow, Magnetization Process of Atacamite: A Case of Weakly Coupled $S = 1/2$ Sawtooth Chains, *Phys. Rev. Lett.* **126**, 207201 (2021).
- [10] A. A. Kulbakov, D. Y. Kononenko, S. Nishimoto, Q. Stahl, A. M. Chakkingal, M. Feig, R. Gumeniuk, Y. Skourski, L. Bhaskaran, S. A. Zvyagin, J. P. Embs, I. Puente-Orench, A. Wildes, J. Geck, O. Janson, D. S. Inosov, and D. C. Peets, Coupled frustrated ferromagnetic and antiferromagnetic quantum spin chains in the quasi-one-dimensional mineral antlerite $\text{Cu}_3\text{SO}_4(\text{OH})_4$, *Phys. Rev. B* **106**, L020405 (2022).
- [11] A. A. Kulbakov, E. Sadrollahi, F. Rasch, M. Avdeev, S. Gaß, L. T. Corredor Bohorquez, A. U. B. Wolter, M. Feig, R. Gumeniuk, H. Poddig, M. Stötzer, F. J. Litterst, I. Puente-Orench, A. Wildes, E. Weschke, J. Geck, D. S. Inosov, and D. C. Peets, Incommensurate and multiple- q magnetic misfit order in the frustrated quantum spin ladder material antlerite $\text{Cu}_3\text{SO}_4(\text{OH})_4$, *Phys. Rev. B* **106**, 174431 (2022).
- [12] H. T. Diep, *Frustrated Spin Systems* (World Scientific Publishing Co, Singapore, 2013).
- [13] O. A. Starykh, Unusual ordered phases of highly frustrated magnets: a review, *Rep. Prog. Phys.* **78**, 052502 (2015).
- [14] Z. Y. Zhao, H. L. Che, R. Chen, J. F. Wang, X. F. Sun, and Z. Z. He, Magnetism study on a triangular lattice antiferromagnet $\text{Cu}_2(\text{OH})_3\text{Br}$, *J. Phys.: Cond. Matter* **31**, 275801 (2019).
- [15] H. Zhang, Z. Zhao, D. Gautreau, M. Raczkowski, A. Saha, V. O. Garlea, H. Cao, T. Hong, H. O. Jeschke, S. D. Mahanti, T. Birol, F. F. Assaad, and X. Ke, Coexistence and Interaction of Spinons and Magnons in an Antiferromagnet with Alternating Antiferromagnetic and Ferromagnetic Quantum Spin Chains, *Phys. Rev. Lett.* **125**, 037204 (2020).
- [16] D. M. Gautreau, A. Saha, and T. Birol, First-principles characterization of the magnetic properties of $\text{Cu}_2(\text{OH})_3\text{Br}$, *Phys. Rev. Mater.* **5**, 024407 (2021).
- [17] T. T. Xiao, Z. W. Ouyang, X. C. Liu, J. J. Cao, Z. X. Wang, and W. Tong, Angular dependence of spin-flop transition in triangular lattice antiferromagnet

- $\text{Cu}_2(\text{OH})_3\text{Br}$, *J. Phys.: Cond. Matter* **34**, 275804 (2022).
- [18] X. G. Zheng, T. Mori, K. Nishiyama, W. Higemoto, H. Yamada, K. Nishikubo, and C. N. Xu, Antiferromagnetic transitions in polymorphous minerals of the natural cuprates atacamite and botallackite $\text{Cu}_2\text{Cl}(\text{OH})_3$, *Phys. Rev. B* **71**, 174404 (2005).
- [19] S. V. Krivovichev, F. C. Hawthorne, and P. A. Williams, Structural complexity and crystallization: the Ostwald sequence of phases in the $\text{Cu}_2(\text{OH})_3\text{Cl}$ system (botallackite–atacamite–clinoatacamite), *Struct. Chem.* **28**, 153 (2017).
- [20] Y. Skourski, M. D. Kuz'min, K. P. Skokov, A. V. Andreev, and J. Wosnitzer, High-field magnetization of $\text{Ho}_2\text{Fe}_{17}$, *Phys. Rev. B* **83**, 214420 (2011).
- [21] R. B. Clover and W. P. Wolf, Magnetic Susceptibility Measurements with a Tunnel Diode Oscillator, *Rev. Sci. Instr.* **41**, 617 (1970).
- [22] S. Ghannadzadeh, J. S. Möller, P. A. Goddard, T. Lancaster, F. Xiao, S. J. Blundell, A. Maisuradze, R. Khasanov, J. L. Manson, S. W. Tozer, D. Graf, and J. A. Schlueter, Evolution of magnetic interactions in a pressure-induced Jahn-Teller driven magnetic dimensionality switch, *Phys. Rev. B* **87**, 241102 (2013).
- [23] Z. Shi, S. Dissanayake, P. Corboz, W. Steinhardt, D. Graf, D. M. Silevitch, H. A. Dabkowska, T. F. Rosenbaum, F. Mila, and S. Haravifard, Discovery of quantum phases in the Shastry-Sutherland compound $\text{SrCu}_2(\text{BO}_3)_2$ under extreme conditions of field and pressure, *Nat. Commun.* **13**, 2301 (2022).
- [24] S. A. Zvyagin, J. Krzystek, P. H. M. van Loosdrecht, G. Dhahlenne, and A. Revcolevschi, High-field ESR study of the dimerized-incommensurate phase transition in the spin-Peierls compound CuGeO_3 , *Physica B* **346-347**, 1 (2004).
- [25] I. Dzyaloshinsky, A thermodynamic theory of 'weak' ferromagnetism of antiferromagnetics, *J. Phys. Chem. Solids* **4**, 241 (1958).
- [26] T. Moriya, Anisotropic Superexchange Interaction and Weak Ferromagnetism, *Phys. Rev.* **120**, 91 (1960).
- [27] M. Oshikawa and I. Affleck, Field-Induced Gap in $S = 1/2$ Antiferromagnetic Chains, *Phys. Rev. Lett.* **79**, 2883 (1997).
- [28] Y. Chen, M. B. Stone, M. Kenzelmann, C. D. Batista, D. H. Reich, and C. Broholm, Phase diagram and spin Hamiltonian of weakly-coupled anisotropic $S = \frac{1}{2}$ chains in $\text{CuCl}_2 \cdot 2((\text{CD}_3)_2\text{SO})$, *Phys. Rev. B* **75**, 214409 (2007).
- [29] E. Turov, A. Kolchanov, and M. Kurkin, *Symmetry and Physical Properties of Antiferromagnetics* (Cambridge International Science Publishing, 2004).
- [30] B. Lake, D. A. Tennant, C. D. Frost, and S. E. Nagler, Quantum criticality and universal scaling of a quantum antiferromagnet., *Nat. Mater.* **4**, 329 (2005).
- [31] R. Coldea, D. A. Tennant, and Z. Tylczynski, Extended scattering continua characteristic of spin fractionalization in the two-dimensional frustrated quantum magnet Cs_2CuCl_4 observed by neutron scattering, *Phys. Rev. B* **68**, 134424 (2003).
- [32] A. I. Smirnov, K. Yu. Povarov, S. V. Petrov, and A. Ya. Shapiro, Magnetic resonance in the ordered phases of the two-dimensional frustrated quantum magnet Cs_2CuCl_4 , *Phys. Rev. B* **85**, 184423 (2012).
- [33] K. Nawa, D. Hirai, M. Kofu, K. Nakajima, R. Murasaki, S. Kogane, M. Kimata, H. Nojiri, Z. Hiroi, and T. J. Sato, Bound spinon excitations in the spin- $\frac{1}{2}$ anisotropic triangular antiferromagnet $\text{Ca}_3\text{ReO}_5\text{Cl}_2$, *Phys. Rev. Research* **2**, 043121 (2020).
- [34] A. G. Gurevich and G. A. Melkov, *Magnetization Oscillations and Waves* (CRC Press, U.K., 1996).
- [35] A. Reinold, L. Berger, M. Raczkowski, Z. Zhao, Y. Kohama, M. Gen, D. I. Gorbunov, Y. Skourski, S. Zherlitsyn, F. F. Assaad, T. Lorenz, and Z. Wang, Magnetization Process of a Quasi-Two-Dimensional Quantum Magnet: Two-Step Symmetry Restoration and Dimensional Reduction, *arXiv*, 2411.09541 (2024).
- [36] S. Toth and B. Lake, Linear spin wave theory for single- Q incommensurate magnetic structures, *J. Phys.: Condens. Matter* **27**, 166002 (2015).